

COMPARATIVE EFFECT OF DIFFERENT NANOPARTICLES ON STRUCTURAL, THERMAL AND BARRIER PROPERTIES OF POLY(ETHYLENE TEREPHTHALATE) IN FOOD PACKAGING SECTOR

Arezoo Ebrahimi¹, Maryam Zabihzadeh Khajavi¹, Shervin Ahmadi², Elahe Foroogi¹, Narges Omid¹, Mehdi Farhoodi¹✉

¹ Department of Food Science and Technology, National Nutrition and Food Technology Research Institute, Faculty of Nutrition Sciences and Food Technology, Shahid Beheshti University of Medical Sciences, Tehran, Iran

² Iran Polymer and Petrochemical Institute, PO Box 14975/112, Tehran, Iran.

✉ Farhoodi@sbmu.ac.ir

<https://doi.org/10.34302/crpfjst/2022.14.1.4>

Article history:

Received:

18 June 2021

Accepted:

18 December 2021

Keywords:

Poly (ethylene terephthalate);

Closite;

Somasif;

Nanocomposite.

ABSTRACT

In the present study, the effect of nanoclay and nanomica on the structural, thermal and barrier properties of poly (ethylene terephthalate) was investigated. The morphology of the papered nanocomposites (Clay and Mica) was illustrated by X-Ray Diffraction (XRD), Transmission electron microscopy (TEM) and Atomic force microscopy (AFM). According to Dynamic Mechanical Thermal Analyzer (DMTA) results, the samples' $\tan\delta$ values ranged from 0.4 to 0.6. The results of Differential scanning calorimetry (DSC) revealed that the incorporation of nanoparticles increased both the crystallization temperature (T_c) and the degree of crystallization (X_c). Then, the higher aspect ratio of nanomica compared to nanoclay led to higher levels of X_c . A significant water vapor permeability decrease (maximum reduction at 1% loading level of nanomica) of nanocomposites was attributed to an increase in the tortuosity of water vapor molecules path diffusing into the nanocomposites. PET/mica nanocomposites presented larger tortuosity factors compared to PET/clay. As a result, improved barrier properties of nanocomposites were obtained in the case of food packaging.

1. Introduction

Over past decades, polymers have been augmented with micro-fillers to obtain higher stiffness and strength, improve fire resistance, or cost reduction. Though, the incorporation of these particles may have some detrimental effects, for instance, opacity and brittleness. Nanoparticles have been used to overcome the restrictions of micro-scale fillers (Müller et al., 2017). In addition, very low loading levels of nanoparticles (<10 wt.%) in comparison to micro-fillers (usually 25-40 wt.%) are required to achieve improvements in nanocomposites (Chouit et al., 2014; Nilagiri Balasubramanian

& Ramesh, 2018; Sravanthi, Mahesh, & Rao, 2021).

Size, shape, structure, specific surface area, concentration and adequate dispersion of nanoparticles can affect the ultimate properties of the nanocomposite (Coetzee, Venkataraman, Militky, & Petru, 2020; Ferdous, Sarker, & Adnan, 2013). There can be three categories of nanoparticles in terms of size and shape to polymer reinforcement. The first nanoparticles possess one dimension in the nanometer scale (≤ 100 nm), such as layered nanographite and platelet-like shaped montmorillonite (nanoclays); the second with two dimensions in

the nano-scale, elongated structures, for instance, carbon nanotubes or fibers; and the third has all three dimensions in the nano-scale such as SiO₂, spherical silica and titanium oxide (Winkler, Notter, Meyer, & Naegeli, 2018).

Several research studies have investigated different effects of nanoparticles on the properties of PET films. The results showed that the incorporation of nanoparticles could increase the crystallization rate of nanocomposites due to the heterogeneous nucleation role of nanoplatelets (Madakbaş, Türk, Şen, & Kahraman, 2017; Papageorgiou et al., 2014). Some research studies have also discussed the effect of nanoparticles on the crystallization and viscoelastic behavior of PET (Ghanbari, Heuzey, Carreau, & Ton-That, 2013; X. Zhang, Zhao, Mohamed, Kuo, & Xin, 2020). On thermal properties of PET nanocomposites, it has been found that the glass transition point of PET nanocomposite could increase (Wang, Wei-huWang, Zhang, Xu, & Li, 2016) or decrease (Lima, Costa, Sousa, Arruda, & Almeida, 2021) or without change (Farhoodi et al., 2012) in comparison with pure polymer.

Nano reinforcements are nano-scale particles that are dispersed into a specific polymer matrix through processing. One of the most important properties is the ratio of the largest to the smallest dimension of nanofiller, known as the aspect ratio (Sahani & Sharma, 2020). High aspect ratios of nanoparticles lead to increased surface areas with improved, reinforcing properties (Dasgupta & Ranjan, 2018; Sahani & Sharma, 2020). In the case of food packaging applications, the aspect ratio has considerable attention in improving packages' boundary properties. Higher aspect ratios make better boundary properties against gasses (oxygen, water vapor, ethylene, etc.). Consequently, because of the sensitivity of some food (for example, oils, dairy products, fruit and vegetables, etc.) to gasses and water, nano-packaging can play a critical role in inhibiting food quality degradation, development of rancid off-flavors, changes in color, shelf life reduction and impair of nutritional quality (Boskovic,

Glisic, Djordjevic, & Baltic, 2019; Pillai & Ray, 2015; C. Zhang et al., 2018).

The properties of the bulk polymer will be significantly affected by changes in the size and number of nanoparticles per unit volume (Luo, Wu, & Zhi, 2016). The relation between aspect ratio, volume percent and barrier property of nanocomposites is shown in equation (1) (Choudalakis & Gotsis, 2009):

$$\frac{P}{P'} = \frac{1}{1 + \frac{1}{2\phi} \cdot \left(\frac{L}{W}\right)} \quad (1)$$

where P is the permeability of nanocomposite, P' is the permeability of neat polymer, ϕ is volume percent, and L/W is the aspect ratio of nanocomposites.

Tortuosity factor (τ) is determined as the distance travelled by a permeant molecule (d') to the thickness of the specimen (d) (see equation 2).

$$\tau = \frac{d'}{d} = 1 + \frac{1}{2\phi} \cdot \left(\frac{L}{W}\right) \quad (2)$$

Therefore, the larger aspect ratio of nanoparticles leads to an increase in the content of d' and, ultimately, enhancement in the polymer's tortuosity factor and barrier properties.

This study aimed to evaluate how nanoparticles with different aspect ratios, including nanoclay and nanomica, at different concentrations (0, 1, 3 and 5% wt.) can affect the structure, thermomechanical and barrier properties of PET nanocomposites.

2. Materials and methods

2.1. Materials

Neat polyethylene terephthalate (PET) (blow molding grade) with an intrinsic viscosity of 0.82 dL/g was purchased from Tondgooyan Petrochemical Company (Iran). Somasif MAE and Closite 20A nanoparticles were provided by CBC Company (Japan) and Southern Clay Co. (USA), respectively. The characteristics of selected nanoparticles (as recorded by the company) have been described in Table 1.

Nanoparticle	Commercial name/type	Shape	Code ^a	Density	Organic modifier
Nano clay	Closite20A	platelet-like	NC	1.77 g/ml	2M2HT ^b
Nano mica	Somasif MAE	platelet-like	NM	1.98 g/ml	MT2EtOH ^c

^a NC= Nanoclays (PET1%NC, PET3%NC and PET5%NC), NM= Nano Mica (PET1%NM, PET3%NM and PET5%NM)

^b 2M2HT: dimethyl, dehydrogenated tallow, quaternary ammonium

^c methyl, tallow, bis-2-hydroxyethyl, quaternary ammonium
(Tallow: ~65% C18; ~30% C16; ~5% C14)

PET was reinforced with 1D platelet-like shape of organo-modified layered silicates (Closite20A) (platelet size approx. 1 x 200 nm) and 1D platelet-like shape of organo-modified layered silicates (Somasif MAE) (platelet size approx. 1 x 200 nm).

2.2. Methods

2.2.1. PET nanocomposites preparation

PET granules and nanoparticles powders were dried overnight at 140°C. The mixing process was developed using a Lab mixer (HAAKE Rheomix 600[®]) at 60 rpm. Further, PET nanocomposites incorporated with 1, 3 and 5 wt. % of both mica and clay nanoparticles were prepared using melt blending in a lab-scale counter-rotating twin-screw extruder (Collin ESC-T10 model). The extruder contained 5 heater zones fixed at 250, 270, 275, 270, 265, and a die zone set at 265°C (with the screw speed of 90 rpm). Before extrusion, nanocomposite components were dried in an oven at 170°C for 5 h. The prepared profiles were water cooled and after that, milled in conventional milling equipment. Pure PET specimen (coded as PET0) was fabricated by the same process (Farhoodi et al., 2012).

2.2.2. DSC analysis

The thermal properties of PET samples were measured by differential scanning calorimeter 200 F3 Maia[®] (NETZSCH, Germany) equipment. Nanocomposite specimens' melting behavior has been investigated using heating and cooling tests in the range of 25-270°C at a heating rate of 10°C/min. The first heating run was utilized to delete the thermal history, and all reported data on the melting properties of the

prepared specimens were obtained from the second heating curve. The degree of crystallinity (X_c) of prepared PET samples were determined by the equation (3):

$$X_c = \left(\frac{\Delta H_m}{\Delta H_{m0}} \right) \times 100 \quad (3)$$

where ΔH_m is the melting enthalpy of the samples, and ΔH_{m0} is the melting enthalpy of 100% crystalline PET ($\Delta H_{m0}=140$ J/g) (Lima et al., 2021).

2.2.3. Transmittance

The transparency of films was measured using a lux meter (Testo 540 pocket-sized lux meter, UK). To do this, the device bubble was placed under an optical source with minimum volatility, and the lux was noted. Then, in stable condition, the specimen was placed on the bubble, and the lux was received. From the two numbers obtained, the transparency of the samples was reported as percentages.

2.2.4. Dynamic mechanical analysis (DMA)

A Polymer Laboratories DMTA (Polymer Laboratories, Loughborough, UK) was employed for DMTA experiments. A frequency of 1 Hz and a temperature range of 25 to 270°C was used with single cantilever bending of samples for these experiments (around 30×10×2 mm³ in size).

2.2.5. X-ray diffraction (XRD)

An X-ray diffractometer (Siemens D5000-Germany) with Cu K α radiation in the wavelength of 1.5409Å (operational tube voltage and current 30 kV and 30 mA, respectively) was used to record the XRD patterns at room temperature. The samples were scanned in 2 θ scan mode by increasing the

temperature from 2 to 80 with a step size of 0.04°C.

In Equation 4, the relation between the angular and layer spacing values according to the Bragg's law is shown.

$$\lambda = 2d \sin \theta \quad (4)$$

where d is spacing between diffraction lattice planes and θ is the measured diffraction angle. The Scherrer equation is widely used to calculate full-width data at half maximum (FWHM) intensity, expected for that average crystallite size:

$$L = \frac{K \cdot \lambda}{\beta_m \cdot \cos \theta} \quad (5)$$

where λ is the X-ray wavelength, β_m is the line width of the 'pure' diffraction profile resulting from small crystallite size, θ is the diffraction angle, and K is a constant almost equal unity and depended on crystallite shape.

2.2.6. Transmission Electron Microscopy (TEM)

Ultra-thin sections of the nanocomposites at a thickness of 70-100 nm were prepared with a microtome (Leica Ultra-cut UCT, Vienna, Austria) using a diamond knife. The morphology of PET/clay and PET/mica nanocomposites were revealed by transmission electron microscopy (TEM, Philips-EM208S electron).

2.2.7. Atomic Force Microscopy (AFM)

A DualScope scanning probe-optical microscope (DME, Denmark) equipped with a DS 95-50-E scanner and an AC probe was used to prepare tapping-mode AFM micrographs. The tapping-mode AFM has been recently developed by changing the cantilever probe's phase angle to create a second image, referred to as the phase-contrast image. During tapping-mode, the phase lag between the cantilever drive frequency and its response can often create significantly more contrast than the topographic image and is sensitive to material surface characteristics, for instance, viscoelasticity, stiffness, and chemical composition. In general,

variations in phase angle through scanning are dependent on energy dissipation during tip-sample interaction and can be a result of variations in topography, tip-sample molecular interactions and deformation at the tip-sample contact (Jiang et al., 2003). In this study, nanoparticles dispersion has been found by the phase images of PET nanocomposites. Measurements were performed in the air at room temperatures. Height and phase images were recorded at the same time.

2.2.8. Water Vapor Permeability Test

The values of water vapor transmission were determined using anhydrous calcium chloride as a desiccant (dish method) according to the ASTM-E 96. Circular trials with a thickness of 0.16 ± 0.01 mm and an area of 28.7 cm^2 were prepared by compression molding then dried at 120°C for 24 h. The water vapor permeability (WVP) was calculated at 30°C and 75% relative humidity (RH). The permeability of water vapor P [$\text{g m} / \text{Pa m}^2 \text{ h}$] is measured from Eq. (6):

$$P = \frac{\frac{m}{t \cdot A}}{\frac{P_s (RH_1 - RH_2)}{100}} \cdot L \quad (6)$$

where m is the weight gain of the polymer film, t is the time for gaining weight, A is the test area, L is the thickness of the film, P_s is the saturation vapor pressure at the test temperature, RH_1 is the relative humidity in the test chamber, RH_2 is the relative humidity at the dry side of the film, which was considered to be zero. Highly dispersed nanoparticles have the ability to increase the tortuosity of the system significantly. According to the Nielsen model, the ratio of permeability of pure polymer to nanocomposite polymer has been defined as the tortuosity factor (Tan & Thomas, 2017).

2.3. Statistical analysis

Data analysis was carried out using SPSS statistical software version 23 (SPSS Inc., Chicago IL). To recognize any significant difference between samples, analysis of variance (two-way ANOVA) followed by Bonferroni test was employed. The level of

significance was set at $p < 0.05$. All tests were run in triplicate.

3. Results and discussion

3.1. Transparency

Regarding the effect of nanoparticles' presence in the polymer structure, maintaining the transparency of the prepared nanocomposites is one of the parameters that should be considered during production. According to the observation of prepared films and the results from lux meter (Table 2), the

highest transparency was observed in neat PET samples ($89.5 \pm 2.24\%$), while the 5% nanomica samples had the minimum values ($61.6 \pm 1.95\%$). The transparency of samples was significantly affected by the type and percentage of nanoparticles ($p < 0.05$). Significant differences were also observed between all nanoparticle levels. The incorporation of nanoclay (NC) in comparison with nanomica (NM) made a minor change in the transparency of the nanocomposites ($p < 0.05$).

Table 2. The effect of nanoparticles on the transparency of the films.

Sample	Transparency (%)	SD
PET0	89.50 ^a	2.24
PET1%NC	81.02 ^b	1.62
PET3%NC	75.00 ^c	2.25
PET5%NC	70.32 ^d	2.25
PET1%NM	72.02 ^e	1.44
PET3%NM	67.91 ^f	2.04
PET5%NM	61.06 ^g	1.95

Appropriate dispersion of clay and mica nanoparticles in 1 wt.% and thoroughly exfoliated structure (according to the result of XRD and TEM) at low loading levels of nanoparticles caused more transparent films. By increasing the amount of nanoparticles in the polymer matrix, the exfoliation morphology is reduced, and the probability of increasing the sizes of the nanoparticles and flocculated structure increased. Consequently, darkening of PET/mica and PET/clay nanocomposite films was observed at the levels of 3 and 5%. Lin et al. (2020) indicated that most nanoparticles have dimensions less than the visible light wavelength, especially clay platelets with exfoliated nanostructures. So, no significant changes in the transparency of the prepared films are expected (Lin, Bilotti, Bastiaansen, & Peijs, 2020). Nevertheless, a significant decrease in the films' transmittance will be

observed when the nanoparticles are not entirely dispersed in the polymer matrix. Other possible reasons are due to the nature of the nanoparticles and the probable crystallization of the prepared nanocomposites (Dadashi, Mousavi, Emam-Djomeh, & Oromiehie, 2014). Considering that the films used in this study entered the cold water immediately after leaving the thermal press, there was no crystallisation chance. Therefore, changing the degree of crystallinity could not be an effective factor in this study's transparency.

3.2. Investigation of thermal properties by DSC

Measurements of glass transition temperature (T_g), crystallization temperature (T_c), enthalpy of crystallization (ΔH_c), melting temperature (T_m), enthalpy of melting (ΔH_m), degree of crystallinity (X_c) and their data analysis are

summarized in Table 3. As seen in Table 3, the reduction in T_g for nanocomposites in comparison to pristine PET is not significant ($p > 0.05$). Unchanged T_g of the nanocomposites could be due to weak cross-linking reaction among PET chains and nanofillers' surface. In the case of PET 5% nanomica, there was almost 3°C decrease in T_g , which could be a result of polymer chains destruction at high shears during the extrusion process in the presence of hard nanomica particles. In several research studies, a decrease in T_g of PET nanocomposites was detected in the presence of MMT (A Greco, Corcione, Strafella, & Maffezzoli, 2010; Antonio Greco, Gennaro, & Rizzo, 2012; Lima et al., 2021). Soon et al. (2009) also reported that molecular weight reduction of polymer after extrusion caused the reduction in T_g ; nevertheless, the decline is not very significant (K. H. Soon et al., 2009). In this study, incorporation of mica and clay nanofillers in PET structure increased both the crystallization temperature (T_c) and the degree of crystallization (X_c). As observed in Table 3, the

nanocomposites containing 1, 3 and 5% nanoparticles have higher crystallization temperatures than neat PET, and the peak width (ΔT_c) for all of them is narrower than neat PET ($p < 0.05$). The narrowest crystallization peak was detected in 3% nanomica, 13.1°C narrower than the ΔT_c of PET0 sample. DSC curves of the cooling and heating process of neat PET, PET/clay and PET/mica nanocomposites are shown in Fig. 1. As identified from the cooling curves (a, c), all nanocomposites' crystallization temperatures are higher than pristine PET. The crystallization peak width reduction can verify the increase of the overall crystallization rate of the produced nanocomposites. Nanocomposites, with 1, 3 and 5% loading of C20A and MAE, showed higher X_c than the PET0 ($p < 0.05$) and the highest X_c was observed at 1 wt.% loading of mica nanoparticles (Table 3). Incorporation of 1% w/w nanoclay and nanomica caused an 11.94% and 16.63% increase in the degree of crystallinity, respectively.

Table 3. The characteristic values of DSC analysis of samples.

Sample	T_g (°C)	T_m (°C)	ΔT_m (°C)	ΔH_m (J/g)	X_c (%)	T_c (°C)	ΔT_c (°C)	ΔH_c (J/g)
PET0	80.5 ^a ± 0.05	249.2 ^a ± 0.1	20.1 ^a ± 0.2	35.48 ^a ± 0.31	33.48 ^a ± 0.2	187.5 ^a ± 0.7	24.3 ^a ± 0.14	37.73 ^a ± 0.3
PET1%NC	80.87 ^a ± 0.09	249.8 ^a ± 0.08	20.8 ^a ± 0.15	48.14 ^b ± 0.13	45.42 ^b ± 0.18	190.2 ^b ± 0.28	20.0 ^b ± 0.56	47.92 ^b ± 0.09
PET3%NC	79.27 ^a ± 0.35	250.3 ^{ab} ± 0.12	19.3 ^b ± 0.24	42.15 ^c ± 0.2	39.77 ^c ± 0.09	192.1 ^c ± 0.14	17.6 ^c ± 0.08	41.70 ^c ± 0.1
PET5%NC	79.25 ^a ± 0.27	251.0 ^b ± 0.2	19.3 ^b ± 0.12	40.32 ^d ± .15	38.05 ^d ± 0.1	192.3 ^c ± 0.42	17.3 ^c ± 0.07	40.35 ^d ± 0.05
PET1%NM	80.08 ^a ± 0.21	245.07 ^c ± 0.2	23.49 ^c ± 0.3	53.10 ^e ± 0.42	50.11 ^e ± 0.21	204.5 ^d ± 0.01	12.54 ^d ± 0.07	46.29 ^e ± 0.12
PET3%NM	79.64 ^a ± 0.3	249.48 ^d ± 0.35	23.12 ^c ± 0.39	44.61 ^f ± 0.09	42.10 ^f ± 0.3	207.60 ^e ± 0.4	11.20 ^f ± 0.04	43.34 ^f ± 0.23
PET5%NM	77.53 ^a ± 0.22	252.60 ^e ± 0.14	25.08 ^d ± 0.12	44.93 ^f ± 0.11	42.40 ^f ± 0.15	209.13 ^f ± 0.6	12.25 ^d ± 0.07	44.84 ^g ± 0.08

^{a-f} significantly different ($p < 0.05$).

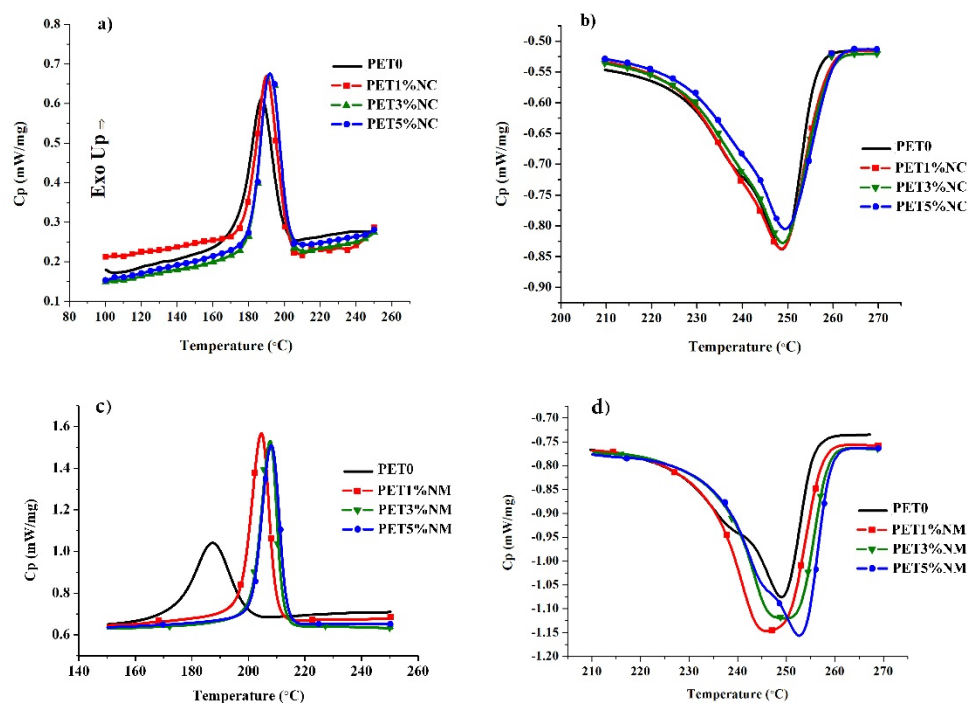


Figure 1. DSC curves of neat PET, PET/clay and PET/mica nanocomposites (a, c) the cooling process, (b, d) the heating process

However, when the content of C20A and MAE reached 3 and 5%, X_c was reduced. The existence of impenetrable crystals on the amorphous polymer region can hinder the diffusion of gases like water vapor through the polymer matrix. The crystallization behavior of nanocomposites is typically related to nanofillers loading levels and their dispersion in the polymer matrix and the relative dominating status of two effects of nanoparticles (nucleation effect and growth restriction effect). Crystallinity degree measurements indicated that the nucleation effect becomes stronger at low nanoparticle contents (1 wt.% C20A and MAE). So, the X_c of these specimens are the highest levels compared to other samples. Whereas, by increasing the nanoparticles loading, the situation could be changed in which the restriction of macromolecules motions effect dominates. In other words, at high loading levels of nanoparticles, the mobility of polymer chain segments is significantly restricted because of the physical barrier properties of nanofillers against the motion of polymer chains (Wan,

Chen, Chua, & Lu, 2004). Thus, the crystallization process of nanocomposites can initiate earlier or at higher temperatures compared to pristine PET. Accordingly, the nucleation rate and, after that, the overall crystallization kinetics promote. The results revealed that synthetic mica on crystallization is more sensible than nanoclays. The higher aspect ratio of nanomica compared to nanoclay could lead to higher levels of X_c . Lima et al. (2021) reported that by incorporation of 2.5% and 7.5% cloisite 20A into PET, higher crystallization temperature in comparison to the neat polymer was obtained (Lima et al., 2021). Another study also revealed an increase in T_c by incorporation of 1, 2 and 3% nanoclay into the PET matrix (Guan et al., 2008). Fig. 1 shows a slight increase in the melting points of clay nanocomposites compared to the neat PET. The melting peaks in PET/mica nanocomposites are broader ($p < 0.05$), especially for PET 5% nanomica ($\Delta T_m = 25.08^\circ\text{C}$ in comparison to 20.1°C for PET 0). The melting point and ΔT_m of clay nanocomposites have been not changed

significantly in comparison with neat PET. This indicates that the crystal forms and the crystal structure of PET have not been changed by incorporation of nanoclay to pet; that is, the melting temperature of PET is constant.

This result is a consequence of solid nanoparticles' presence leading to broader crystallite size distribution and imperfections in the crystallite growth process. Therefore, different sizes of the crystallites with different thermal stabilities formed in nanocomposites can widen the melting peaks.

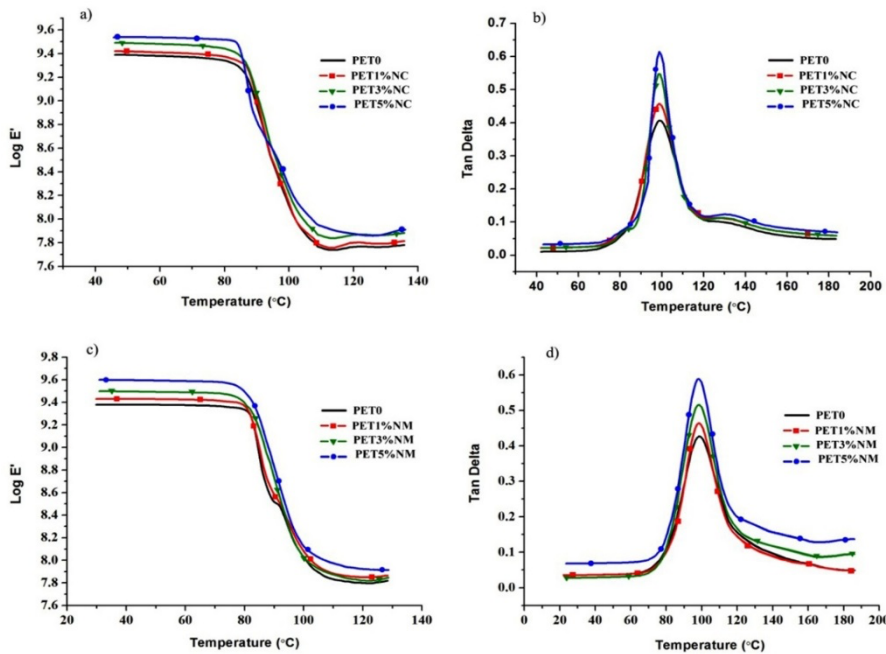


Figure 2(a, c) Storage modulus (E') and (b, d) $\tan\delta$ of neat PET and its nanocomposites

As can be seen in Table 4, $\tan\delta$ values of the obtained samples are in the range of 0.4 - 0.6, indicating that neat PET sample and PET nanocomposites specimens behave like elastic solids more than viscous liquids. The position of $\tan\delta$ peak does not alter significantly for PET/clay and PET/mica nanocomposites compared to PET0 specimens (indicating insignificant changes in T_g values). According to the data analysis, the difference between neat PET and 5% nanocomposites was significant ($p < 0.05$), but the type of nanoparticles made no significant difference between $\tan\delta$ values. By increasing the nanoparticles loading, the $\tan\delta$ peak magnitudes enhance. It can verify that the

3.3. Dynamic mechanical analysis

Fig. 2 (a, c) display the storage modulus (E') and (b, d) $\tan\delta$ of PET/clay and PET/mica nanocomposites against temperature, respectively. $\tan\delta$ indicates the relative significance of both viscous and elastic behaviors of materials, whereby $\tan\delta < 1$ exhibits stronger elastic behavior and materials may behave like solids. While, $\tan\delta > 1$ exhibits stronger viscous behavior and materials' behavior is like liquids more (Bertolo, Martins, Horn, Brenelli, & Plepis, 2020).

pure PET has lower damping capability in comparison with the prepared nanocomposites, and this reduction is more significant for nanocomposite comprising 5 wt.% nanoparticles.

As found, the mean storage modulus varied between 2.15 to 3.90 GPa at 40°C and 0.06 to 0.083 GPa at 140°C depending on the loading of nanofillers from 0 to 5 wt.%. Analysis of our finding showed a significant difference in storage modulus between all treatments at 40°C ($p < 0.05$), but no difference was observed at 140°C ($p > 0.05$). This increasing trend is more sensible in PET/mica.

Table 4. E' at 40°C and 140°C and Tanδ peak values for the neat PET and PET/clay and PET/mica nanocomposites.

Sample	E' at 40 °C (GPa)	E' at 140 °C (GPa)	temp of tanδ at peak (°C)	Tan δ peak value
PET0	2.15 ^a ± 0.2	0.060 ^a ± 0.01	98.76 ^a ± 0.1	0.406 ^a ± 0.13
PET1%NC	2.63 ^b ± 0.1	0.061 ^a ± 0.02	98.50 ^a ± 0.15	0.457 ^a ± 0.1
PET3%NC	3.09 ^c ± 0.11	0.073 ^a ± 0.01	98.57 ^a ± 0.09	0.547 ^{ab} ± 0.07
PET5%NC	3.38 ^d ± 0.3	0.073 ^a ± 0.025	98.59 ^a ± 0.14	0.614 ^b ± 0.06
PET1%NM	2.63 ^e ± 0.12	0.07 ^a ± 0.01	98.36 ^a ± 0.1	0.464 ^a ± 0.1
PET3%NM	3.14 ^f ± 0.2	0.066 ^a ± 0.01	98.79 ^a ± 0.08	0.515 ^{ab} ± 0.12
PET5%NM	3.90 ^g ± 0.15	0.083 ^a ± 0.03	97.80 ^a ± 0.1	0.588 ^b ± 0.07

^{a-f} significantly different (p< 0.05).

Soon et al. (2009) reported that the modulus, particularly above the glass transition, was enhanced by the incorporation of 1, 2 and 5% synthetic mica (Somasif MTE and Somasif MAE) to PET matrices (K. H. Soon et al., 2009). The formation of a network structure among polymer chains and nanoparticles leads to increased storage modulus beyond the T_g point, which enhances the rigidity of the nanocomposites. Other research studies have also reported this fashion (Francis, Joy, Aparna, & Vijayan, 2014; Majdzadeh-Ardakani, Zekriardehani, Coleman, & Jabarin, 2017).

3.4. X-Ray Diffraction (XRD)

To reveal information about Intercalation/exfoliation of PET/clay and

PET/mica Wide-angle XRD (WAXD) measurements on neat PET, pure nanofillers and nanocomposites were carried out. Table 5 summarizes the parameters of XRD curves. The d-spacing values of the PET/mica, PET/clay and nanocomposite sheets were calculated by the Bragg equation. The performance of filling is obviously dependent on the larger interlayer distance of nanoparticles in PET nanocomposites. The polymer chains need to be inserted within the interlayer of the nanoparticle structure to formation of intercalated or exfoliated structures in which an efficient interaction among nanoparticles and polymer matrix is necessary.

Table 5. Values of 2theta and d-spacing for PET nanocomposites.

	2θ	d-spacing (nm)
Nanoclay Powder	5.712	1.53
PET1%NC	2.58	3.50
PET3%NC	3.13	2.85
	5.875	1.51
PET5%NC	3.038	2.96
	5.639	1.56
Nanomica Powder	4.82	1.83
PET1%NM	5.84	1.51
PET3%NM	2.68	3.29
	5.91	1.49
PET5%NM	2.65	3.33
	5.81	1.52

Fig. 3 (a, b) demonstrates the WAXD profiles for the PET/clay and PET/mica nanocomposites, respectively. A mixed morphology of intercalated/exfoliated structure has been formed in all nanocomposites. For nanoclay powder, a peak emerged at about $2\theta = 5.712$ ($d = 1.53$ nm), confirming the basal interlayer spacing of the clay. The maximum decrease in the 2θ value obtained in the systems incorporated with 1% of nano-clays, which corresponds with semi-exfoliation (exfoliation of a certain number of tactoids). A shift to lower angles of the characteristic diffraction peak in 3 and 5 wt.% PET/clay suggests an increase in interlayer spacing of the clay, which is referred to as intercalation. At 1 wt.% Cloisite, the organoclay layers have been randomly dispersed in the polymer (for instance, exfoliated). While increasing the concentration of Cloisite to 3 and 5% suggests intercalated to exfoliated structure in which polymer molecules have entered the distance between organoclay layers.

As seen in Fig. 3b, at PET 1% nanomica, there seems to be a peak at $2\theta < 2$, which has not been revealed in the WAXD analysis. The presence of this peak can be a result of more opening of mica layers at low loading levels. The presence of the peaks at about $2\theta = 2.68$ ($d = 3.29$ nm) for PET 3% nanomica and $2\theta = 2.65$ ($d = 3.33$ nm) for PET 5% nanomica can indicate the opening of the mica layers by polymer chains and formation of intercalation structure. Nevertheless, WAXD should not be used as a stand-alone procedure for the characterization of polymer nanocomposites. In some cases (for instance, large amounts of clay, random orientation of the layers, inhomogeneous distribution of surfactant in the interlayer space or a distribution of interlayer distance) it may lead to a misleading interpretation of the nanostructure. For these reasons, it is recommended that the results of this test be compared with direct observations of the layers by Transmission Electron Microscopy (TEM) or Atomic Force Microscopy (AFM) (K. H. Soon et al., 2009).

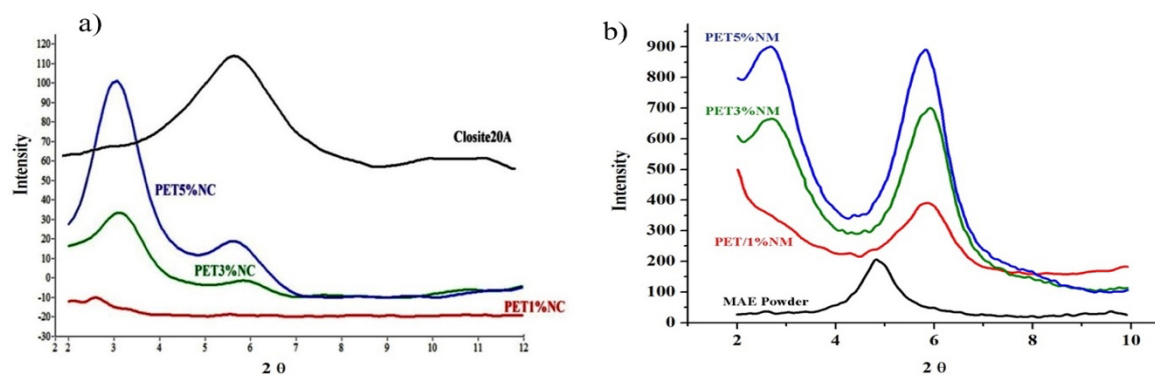


Figure 3. WAXD profiles for Cloisite20A powder and PET/clay (a) and MAE powder and PET/mica nanocomposites (b)

3.5. Transmission Electron Microscopy (TEM)

The TEM micrographs confirm the results of WAXD analysis. TEM micrographs of nanocomposites containing 1 and 3 wt.% nanoclay and nanomica are shown in Fig. 4. The individual delaminated silicate layers especially

nanoclay marked in a circle in Fig. 4b. In Fig. 4 (c, d), micrographs of PET/mica nanocomposites are shown. As can be seen, when the content of nanomica is 1%, the mica layers are completely dispersed in the polymer matrix, and the exfoliated structure is obtained, whereas 3% nanomica gives

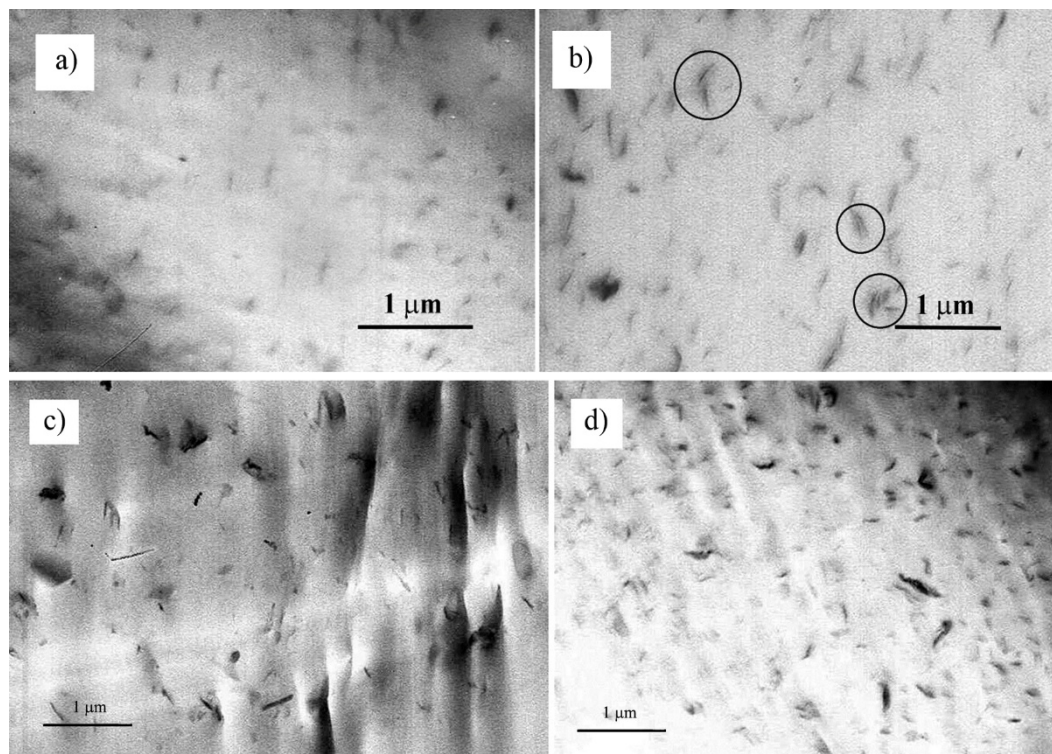


Figure 4. TEM micrographs 1 (a) and 3% (b) nanoclay and 1 (c) and 3% (d) nanomica

detected at 1%wt. Cloisite revealed a more exfoliated structure. A partially exfoliated/intercalated structure with dispersed tactoids for 3% Cloisite was observed. Intercalated/exfoliated structures of 3%

intercalated/exfoliated morphology. The results of the dispersion of nanoparticles in our micrographs are in accordance with previous investigations (K. Soon et al., 2012; K. H. Soon et al., 2009).

3.6. Atomic Force Microscopy (AFM)

The height and phase images of PET nanocomposites are illustrated in Fig. 5 and 6. As shown, phase In Fig. 6, micrographs of 1% PET/mica nanocomposites are shown. As can be seen, when the content of nanomica is 1% (Fig. 6a), the mica layers are completely dispersed in

the polymer matrix, and the exfoliated structure is obtained, whereas 3% nanomica gives intercalated/exfoliated morphology (Fig. 6b). The results of the dispersion of nanoparticles in our micrographs are in accordance with previous investigations (Bizarria et al., 2007; K. H. Soon et al., 2009).

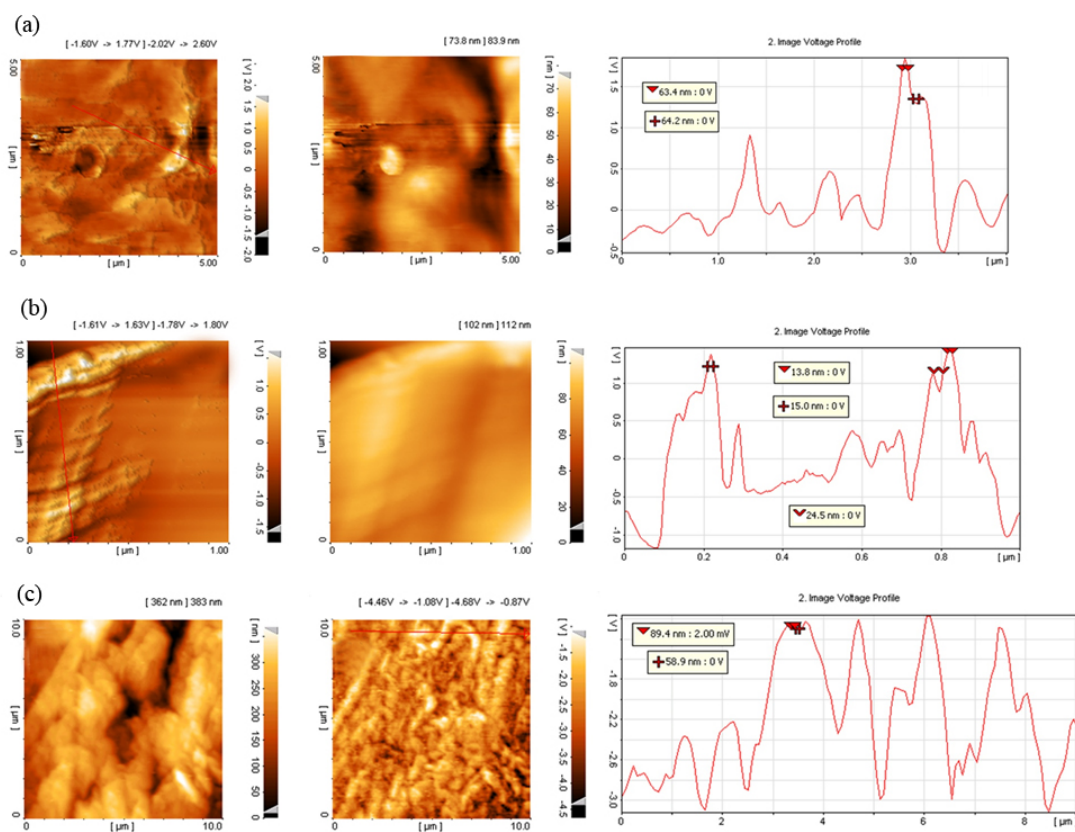


Figure 5. The height and phase images of PET 1% wt. (a), 3% wt. (b) and 5% wt. (c) nanoclay

3.7. Water Vapor Permeability (WVP)

Since water is one of the most critical factors in food spoilage reactions, water vapor transmission rate (WVTR) and water vapor permeability (WVP) are the key properties in polymeric food packaging. WVTR and WVP of nanocomposite films are influenced by various factors, including hydrophilicity and hydrophobicity of the components, nanocomposites preparation method, type and distribution of additives, tortuosity and ultimately order in the polymer structure (Sarfranz, Gulin-Sarfranz, Nilsen-Nygaard, & Pettersen, 2021). The distance travelled by a permeant molecule in the polymer matrix is known as the tortuosity factor. The decrease in WVP of nanocomposites is attributed to an increase in the tortuosity of water vapor molecules path diffusing into the

nanocomposites (Farhoodi, Mohammadifar, Mousavi, Sotudeh-Gharebagh, & Emam-Djomeh, 2017; Saxena et al., 2020). The increased tortuosity of water vapor molecules leads to improved barrier properties of nanocomposites.

The results of measuring the permeability of pure PET films and their nanocomposites are shown in Fig. 7a. As can be seen, each of the nanoparticles has different behaviors. The presence of nanoparticles led to a significant permeability decrease of polymer matrix with a maximum reduction of 64% in 1% PET/mica nanocomposite compared to neat PET. As presented in Fig. 7b, PET/mica nanocomposites have larger tortuosity factors than PET/clay. According to data analysis, there was a significant difference between type and the percentage of nanoparticles on WVP and

tortuosity factor of PET/clay and PET/mica nanocomposites ($p < 0.05$). As a result, nanomica had a more significant effect on reducing permeability and increasing tortuosity factor

than nanoclay. As previously mentioned, significant differences were observed at all levels, especially at 1% wt nanoparticles.

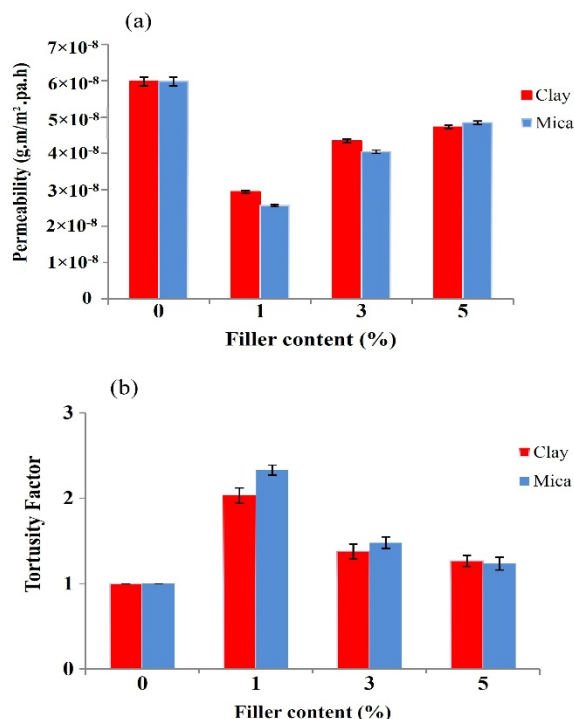


Figure 7. Permeability and tortuosity factor of neat PET films and their nanocomposites

In the case of food packaging, the incorporation of high aspect ratio nanoparticles could increase the tortuosity factor. This factor is a function of the aspect ratio of nanoparticles and the nanofiller volume fraction in the composite. Platelet-like nanoparticles can particularly affect barrier properties of a polymer. Their performance is improved when their degree of exfoliation and their aspect ratio increased (Crisuelo, Gavara, & Hernández-Muñoz, 2015; Yeh et al., 2020).

As previously mentioned, and was observed in our obtained results of XRD, TEM, and AFM, low loading levels of nanoparticles (1% wt.) have been randomly dispersed in the polymer matrix. Therefore, a typical exfoliated structure was formed, and the maximum WVP properties

happened. While at higher loading levels of nanoparticles, the ratio of intercalated to exfoliated structure increased. At high loading levels, the probability of increasing the nanoparticles sizes and flocculated structure increased. In similar research studies, the WVP was significantly reduced for PET nanocomposites; moreover, exfoliated structure improved polymer properties compared to intercalation morphology (Antonio Greco, Esposito Corcione, & Maffezzoli, 2010).

High aspect ratios of nanoparticles could provide large surface areas with better reinforcing effects. A higher aspect ratio of nanoparticles enhances the tortuosity factor. Therefore, due to the more significant aspect ratio of nanomica compared to nanoclay, the

tortuosity factor improved more, particularly at 1% nanoparticles loading levels. Besides, diffusion of moisture is prevented by impermeable crystals, especially at 1 wt% contributed to higher X_c .

4. Conclusions

In this study, the effect of incorporating different levels of nanoclay and nanomica with varying ratios of aspect into the PET matrix on the characteristics of prepared nanocomposites and their influence on barrier properties was investigated. PET/clay and PET/mica nanocomposites were prepared via melt blending. For all the prepared nanocomposites, transparency decreased significantly with increasing nanoparticle content. In addition, nanomica compared to nanoclay made more significant changes in the polymer matrix's transparency. The observations of XRD, TEM, and AFM showed that the exfoliation morphology is reduced by increasing the amount of nanoparticles in the polymer matrix. The probability of increasing the nanoparticles sizes and flocculated structure increased. Consequently, darkening of PET/mica and PET/clay nanocomposite films was observed at the levels of 3 and 5%. According to DSC, the addition of mica and clay nanoparticles in PET structure increased both the crystallization temperature (T_c) and the degree of crystallization (X_c). As a result, the stiffer structure with reduced amorphous regions compared with pure PET was obtained, which increased the tortuosity factor that led to the improvement of barrier properties. Furthermore, the results revealed that the higher aspect ratio of nanomica compared to nanoclay led to higher X_c levels. DMTA results showed an insignificant reduction in T_g for nanocomposites in comparison to pure PET. The magnitudes of $\tan\delta$ peak in prepared nanocomposites enhanced, which can verify that the pure PET has lower damping capability than nanocomposites. This reduction is more significant for nanocomposite containing 5 wt.% nanoparticles. Concerning barrier properties in food packaging, it was observed that the presence of high aspect ratio nanoparticles in the

PET matrix decreased WVP and increased the tortuosity factor. In other words, the increased tortuosity of water vapor molecules led to improved barrier properties of nanocomposites. PET/mica nanocomposites have larger tortuosity factors than PET/clay due to the higher aspect ratio of mica nanoparticles. Taken all the above data together, incorporation of higher aspect ratio nanoparticles, particularly at low loading levels, can significantly reinforce the thermomechanical and barrier properties of the PET matrix.

5. References

- Bertolo, M. R., Martins, V. C., Horn, M. M., Brenelli, L. B., & Plepis, A. M. (2020). Rheological and antioxidant properties of chitosan/gelatin-based materials functionalized by pomegranate peel extract. *Carbohydrate polymers*, 228, 115386.
- Bizarria, M. T., Giraldo, A. L. d. M., de Carvalho, C. M., Velasco, J. I., d'Ávila, M. A., & Mei, L. H. (2007). Morphology and thermomechanical properties of recycled PET–organoclay nanocomposites. *Journal of applied polymer science*, 104(3), 1839-1844.
- Boskovic, M., Glisic, M., Djordjevic, J., & Baltic, M. Z. (2019). Nanotechnology and plant extracts as a future control strategy for meat and milk products. In *Plant nanobionics* (pp. 201-253): Springer.
- Cerisuolo, J. P., Gavara, R., & Hernández-Muñoz, P. (2015). Diffusion modeling in polymer–clay nanocomposites for food packaging applications through finite element analysis of TEM images. *Journal of Membrane Science*, 482, 92-102.
- Choudalakis, G., & Gotsis, A. (2009). Permeability of polymer/clay nanocomposites: a review. *European polymer journal*, 45(4), 967-984.
- Chouit, F., Guellati, O., Boukhezar, S., Harat, A., Guerioune, M., & Badi, N. (2014). Synthesis and characterization of HDPE/N-MWNT nanocomposite films, *Nanoscale Research Letters*, 9.

- Coetzee, D., Venkataraman, M., Militky, J., & Petru, M. (2020). Influence of nanoparticles on thermal and electrical conductivity of composites. *Polymers*, 12(4), 742.
- Dadashi, S., Mousavi, S. M., Emam-Djomeh, Z., & Oromiehie, A. (2014). Functional properties of biodegradable nanocomposites from poly lactic acid (PLA). *International Journal of Nanoscience and Nanotechnology*, 10(4), 245-256.
- Dasgupta, N., & Ranjan, S. (2018). Nanotechnology in food packaging. *An Introduction to Food Grade Nanoemulsions*, 129-150.
- Farhoodi, M., Dadashi, S., Mousavi, S. M. A., Sotudeh-Gharebagh, R., Emam-Djomeh, Z., Oromiehie, A., & Hemmati, F. (2012). Influence of TiO₂ Nanoparticle Filler on the Properties of PET and PLA Nanocomposites. *Polymer Korea*, 36(6), 745-755.
- Farhoodi, M., Mohammadifar, M. A., Mousavi, M., Sotudeh-Gharebagh, R., & Emam-Djomeh, Z. (2017). Migration kinetics of ethylene glycol monomer from pet bottles into acidic food simulant: effects of nanoparticle presence and matrix morphology. *Journal of Food Process Engineering*, 40(2), e12383.
- Ferdous, S. F., Sarker, M. F., & Adnan, A. (2013). Role of nanoparticle dispersion and filler-matrix interface on the matrix dominated failure of rigid C60-PE nanocomposites: A molecular dynamics simulation study. *Polymer*, 54(10), 2565-2576.
- Francis, R., Joy, N., Aparna, E., & Vijayan, R. (2014). Polymer grafted inorganic nanoparticles, preparation, properties, and applications: a review. *Polymer Reviews*, 54(2), 268-347.
- Ghanbari, A., Heuzey, M.-C., Carreau, P. J., & Ton-That, M.-T. (2013). Morphological and rheological properties of PET/clay nanocomposites. *Rheologica Acta*, 52(1), 59-74.
- Greco, A., Corcione, C. E., Strafella, A., & Maffezzoli, A. (2010). Analysis of the structure and mass transport properties of clay nanocomposites based on amorphous PET. *Journal of applied polymer science*, 118(6), 3666-3672.
- Greco, A., Esposito Corcione, C., & Maffezzoli, A. (2010). Water vapor permeability of clay nanocomposites based on amorphous PET. Paper presented at the Defect and Diffusion Forum.
- Greco, A., Gennaro, R., & Rizzo, M. (2012). Glass transition and cooperative rearranging regions in amorphous thermoplastic nanocomposites. *Polymer International*, 61(8), 1326-1333.
- Guan, G., Li, C., Yuan, X., Xiao, Y., Liu, X., & Zhang, D. (2008). New insight into the crystallization behavior of poly (ethylene terephthalate)/clay nanocomposites. *Journal of Polymer Science Part B: Polymer Physics*, 46(21), 2380-2394.
- Jiang, Y., Zhou, J.-J., Li, L., Xu, J., Guo, B.-H., Zhang, Z.-M., Cheung, Z.-L. (2003). Surface properties of poly (3-hydroxybutyrate-co-3-hydroxyvalerate) banded spherulites studied by atomic force microscopy and time-of-flight secondary ion mass spectrometry. *Langmuir*, 19(18), 7417-7422.
- Lima, J. C., Costa, A. R. M., Sousa, J. C., Arruda, S. A., & Almeida, Y. M. (2021). Thermal behavior of polyethylene terephthalate/organoclay nanocomposites: investigating copolymers as matrices. *Polymer Composites*, 42(2), 849-864.
- Lin, Y., Bilotti, E., Bastiaansen, C. W., & Peijs, T. (2020). Transparent semi-crystalline polymeric materials and their nanocomposites: A review. *Polymer Engineering & Science*, 60(10), 2351-2376.
- Luo, D., Wu, L., & Zhi, J. (2016). Nanocomposite for food encapsulation packaging. In *Encapsulations* (pp. 421-454): Elsevier.
- Madakbaş, S., Türk, Z., Şen, F., & Kahraman, M. V. (2017). Thermal and morphological properties of organo modified nanoclay/polyethylene terephthalate composites. *Journal of Inorganic and*

- Organometallic Polymers and Materials*, 27(1), 31-36.
- Majdzadeh-Ardakani, K., Zekriardehani, S., Coleman, M. R., & Jabarin, S. A. (2017). A novel approach to improve the barrier properties of PET/clay nanocomposites. *International Journal of Polymer Science*.
- Müller, K., Bugnicourt, E., Latorre, M., Jorda, M., Sanz, Y. E., Lagaron, J. M., Zuzana Scheuerer 1, S. C. a. M. S. (2017). Review on the processing and properties of polymer nanocomposites and nanocoatings and their applications in the packaging, automotive and solar energy fields. *nanomaterials*, 7(74).
- Nilagiri Balasubramanian, K. B., & Ramesh, T. (2018). Role, effect, and influences of micro and nano-fillers on various properties of polymer matrix composites for microelectronics: A review. *Polymers for Advanced Technologies*, 29(6), 1568-1585.
- Papageorgiou, G. Z., Karandrea, E., Giliopoulos, D., Papageorgiou, D. G., Ladavos, A., Katerinopoulou, A., Bikiaris, D. N. (2014). Effect of clay structure and type of organomodifier on the thermal properties of poly (ethylene terephthalate) based nanocomposites. *Thermochimica acta*, 576, 84-96.
- Pillai, S. K., & Ray, S. S. (2015). Inorganic-organic hybrid polymers for food packaging. *Functional Polymers in Food Science*, 281.
- Sahani, S., & Sharma, Y. C. (2020). Advancements in applications of nanotechnology in global food industry. *Food Chemistry*, 128318.
- Sarfraz, J., Gulin-Sarfraz, T., Nilsen-Nygaard, J., & Pettersen, M. K. (2021). Nanocomposites for Food Packaging Applications: An Overview. *Nanomaterials*, 11(1), 10.
- Saxena, D., Jana, K. K., Soundararajan, N., Katiyar, V., Rana, D., & Maiti, P. (2020). Potency of nanolay on structural, mechanical and gas barrier properties of poly (ethylene terephthalate) Nanohybrid. *Journal of Polymer Research*, 27(2), 1-9.
- Soon, K., Harkin-Jones, E., Rajeev, R. S., Menary, G., Martin, P. J., & Armstrong, C. G. (2012). Morphology, barrier, and mechanical properties of biaxially deformed poly (ethylene terephthalate)-mica nanocomposites. *Polymer Engineering & Science*, 52(3), 532-548.
- Soon, K. H., Harkin-Jones, E., Rajeev, R. S., Menary, G., McNally, T., Martin, P. J., & Armstrong, C. (2009). Characterisation of melt-processed poly (ethylene terephthalate)/synthetic mica nanocomposite sheet and its biaxial deformation behaviour. *Polymer International*, 58(10), 1134-1141.
- Sravanthi, K., Mahesh, V., & Rao, B. N. (2021). Influence of micro and nano carbon fillers on impact behavior of GFRP composite materials. *Materials Today: Proceedings*, 37, 1075-1078.
- Tan, B., & Thomas, N. L. (2017). Tortuosity model to predict the combined effects of crystallinity and nano-sized clay mineral on the water vapour barrier properties of polylactic acid. *Applied Clay Science*, 141, 46-54.
- Wan, T., Chen, L., Chua, Y. C., & Lu, X. (2004). Crystalline morphology and isothermal crystallization kinetics of poly (ethylene terephthalate)/clay nanocomposites. *Journal of applied polymer science*, 94(4), 1381-1388.
- Wang, Y.-h., Wei-huWang, Zhang, Z., Xu, L., & Li, P. (2016). Study of the glass transition temperature and the mechanical properties of PET/modified silica nanocomposite by molecular dynamics simulation. *European Polymer Journal*, 75, 36-45.
- Winkler, H. C., Notter, T., Meyer, U., & Naegeli, H. (2018). Critical review of the safety assessment of titanium dioxide additives in food. *Journal of nanobiotechnology*, 16(1), 1-19.
- Yeh, S. K., Su, C. C., Huang, J. M., Ke, M. Q., Bogale, D., Anbarasan, R., Wang, S. F. (2020). Fabrication of polystyrene/carbon nanocomposites with superior mechanical

properties. *Polymer Engineering & Science*, 60(8), 2046-2056.

Zhang, C., Li, W., Zhu, B., Chen, H., Chi, H., Li, L., Xue, J. (2018). The quality evaluation of postharvest strawberries stored in nano-Ag packages at refrigeration temperature. *Polymers*, 10(8), 894.

Zhang, X., Zhao, S., Mohamed, M. G., Kuo, S.-W., & Xin, Z. (2020). Crystallization behaviors of poly (ethylene terephthalate)(PET) with monosilane isobutyl-polyhedral oligomeric silsesquioxanes (POSS). *Journal of materials science*, 55(29), 14642-14655.